

Vanishing threshold in depolarization of correlated opinions on social networks

Jaume Ojer,¹ Michele Starnini,^{1,2,*} and Romualdo Pastor-Satorras^{1,†}

¹*Departament de Física, Universitat Politècnica de Catalunya, Campus Nord, 08034 Barcelona, Spain*

²*CENTAI Institute, 10138 Turin, Italy*

(Dated: June 5, 2023)

The process of opinion depolarization is assumed to be mediated through social networks, where interacting individuals reciprocally exert social influence leading to a consensus. While network topology plays a decisive role in many networked dynamical processes, its effect on depolarization dynamics remains unclear. Here, we show that, in a recently proposed opinion depolarization model, the threshold of the transition from correlated and polarized opinions to consensus can vanish on heterogeneous social networks. Our theoretical findings are validated by running numerical simulations on both synthetic and real social networks, confirming that a polarized yet heterogeneously connected population can reach a consensus even in the presence of weak social influence.

The emergence of opinion polarization, which usually refers to the presence of two groups in a population holding opposite and potentially extreme opinions [1], can have a negative impact on society, providing a breeding ground for the dissemination of harmful misinformation [2]. Consequently, researchers from distinct scientific disciplines have embarked on studying different mechanisms that could potentially reduce opinion polarization, a process referred to as *depolarization* in the literature [3, 4]. Given the limited availability of reliable data on opinions spanning an extended period, most studies have concentrated on a theoretical understanding of opinion depolarization [5–7].

Several modeling efforts have explored various mechanisms underlying the opinion formation process, such as homophily [8, 9], bounded confidence [10, 11], or opinion rejection [12, 13]. While earlier studies typically focused on a single topic [14, 15], researchers recently have proposed novel modeling frameworks to address the case of multi-dimensional opinions [16–18], where opinions can vary across different topics. Notably, when multiple topics are considered, correlations between opinions may arise [19–22]. For instance, racism and the stereotype of blacks as violent individuals may be related to gun ownership and opposition to gun control policies in US whites [23].

One possibility to meaningfully study opinion dynamics regarding two interdependent topics is to represent them in the polar plane [24], where the angle φ represents the orientation of an individual with respect to both topics and the radius ρ expresses his/her attitude strength or conviction. Such a polar representation allows for a natural interpretation of opinion polarization, typically represented by groups with opposite orientations φ in the polar plane (regardless of the conviction value ρ) [25]. In particular, two individuals holding contrary opinions with respect to two topics will be represented by opposite orientations, maximally separated by an angle π . On the other hand, consensus, representing individuals converging towards a common ground [26], is reached when agents align their orientation to a common value. The angular distribution

$P(\varphi)$ permits to easily identify correlations between opinions: when opinions are polarized and strongly correlated, $P(\varphi)$ is characterized by two peaks (bimodal distribution), corresponding to the opposite ideologies at play. For instance, political ideology could be defined by two major axes, the economic axis (left vs right) measuring the desire for state intervention in the economy, and the social axis (libertarian vs authoritarian) measuring the desire for personal freedom [27]. Within this context, the polar representation intuitively shows that a population characterized by two groups with opposite orientations (such as left and libertarian vs right and authoritarian) is more polarized than two groups with a smaller distance, measured by the orientation difference (left vs right, both libertarian).

The process of opinion depolarization can be represented as a phase transition from an initially polarized opinion state to a consensus, typically due to the social influence exerted by individuals on their peers [28–30]. When multiple topics are taken into account, the correlations between opinions may play an important role [31], triggering in some cases an explosive depolarization transition [24]. Understanding the nature of such a transition, determined by the modeling framework, is crucial to determine under which conditions the population is able to reduce opinion polarization more effectively. These conditions may include the connectivity of the social network underlying the process of opinion formation, which is generally assumed to be mediated by social interactions. While the network topology has been shown to play a pivotal role in different networked dynamical processes [32], its effect in depolarization models has not been explored yet.

In this paper, we address this important open question by analytically studying a recently proposed opinion depolarization model, the so-called social compass model, in which two interdependent topics are represented in the polar plane [24]. We assume polarized and strongly correlated initial opinions, as is reported through different experiments like empirical opinion surveys regarding controversial topics [4, 24, 33]. We then contrast two different theoretical approaches to investigate the conditions for the emergence of consensus. We show that, when a non-trivial connectivity is assumed among the interacting agents, the depolarization threshold is entirely determined by the network topology. For heterogeneous (thus realistic) social networks, we demonstrate a vanishing threshold for the social influence needed to trigger the depolarization

* Corresponding author: michele.starnini@upc.edu

† Corresponding author: romualdo.pastor@upc.edu

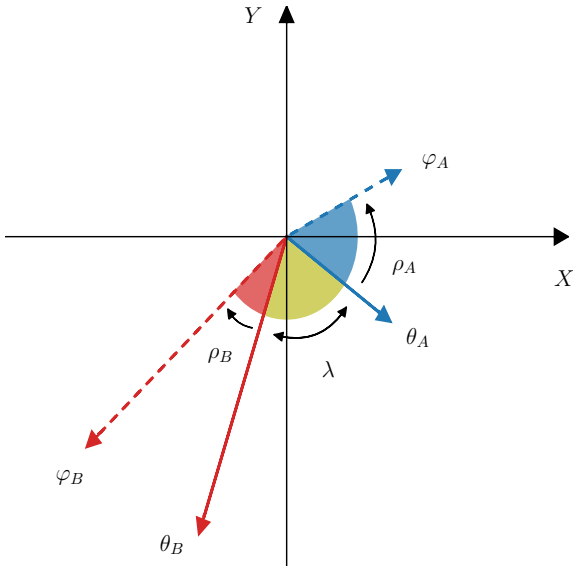


Figure 1. **Illustrative scheme of the social compass model.** We sketch two connected individuals, A and B , holding conviction ρ_A and ρ_B , and initial orientation φ_A and φ_B , respectively, towards two distinct topics X and Y . Their orientations θ_A and θ_B evolve in time as the result of two competing forces: they tend to align with their initial orientation proportionally to their conviction, and they are subject to reciprocal social influence proportionally to the coupling strength λ .

of the population. Our theoretical findings are validated by running extensive simulations of the depolarization model on both synthetic and empirical social networks, confirming that the initial polarized state is very susceptible to disappear even when social influence among individuals is very weak.

The social compass model. Let us consider a set of N agents, each one endowed with a conviction, ρ_i , and a preferred orientation, φ_i . The evolution of the orientation in time, $\theta_i(t)$, is determined by two competing factors: individuals are i) subject to the social influence of their peers and ii) stubborn to their initial, preferred orientation $\theta_i(0) = \varphi_i$. This dynamics can be modeled by the set of ordinary differential equations [24]

$$\dot{\theta}_i(t) = \rho_i \sin[\varphi_i - \theta_i(t)] + \lambda \sum_{j=1}^N a_{ij} \sin[\theta_j(t) - \theta_i(t)]. \quad (1)$$

The first term in Eq. (1) models the tendency of individuals to remain close to their preferred orientation, which we assume to be proportional to their conviction, considered constant in time. The second term accounts for the social influence of peers, mediated by a social network [34] with adjacency matrix a_{ij} [35], taking the value $a_{ij} = 1$ when agents i and j are socially connected and $a_{ij} = 0$ otherwise. The social influence, quantified by the coupling constant λ , tends to make the orientation of an agent aligned to the orientation of their neighbors. Figure 1 illustrates the basic mechanisms of the social compass model.

The model is completely defined by the probability distributions $P(\rho)$ and $P(\varphi)$ that a randomly chosen agent has

conviction ρ and initial orientation φ , respectively, which we assume to be statistically independent. Here, we focus on a power-law form of the conviction distribution, defined in the interval $[0, 1]$,

$$P(\rho) = (\alpha + 1)\rho^\alpha, \quad (2)$$

with $\alpha \geq 0$, and a bimodal distribution of initial orientations,

$$P(\varphi) = \frac{1}{2} [\delta(\varphi) + \delta(\varphi + \pi)], \quad (3)$$

aimed at describing maximally correlated initial opinions.

In the absence of social interactions ($\lambda = 0$), Eq. (1) leads to the steady state $\theta_i = \varphi_i$, i.e., every agent is aligned with their preferred orientation, which is assumed to be a polarized state. For large λ , on the other hand, social influence prevails over stubbornness and a depolarized (consensus) state emerges, with all the agents having the same average orientation $\theta_i \simeq \psi$. Therefore, the model exhibits a phase transition from a polarized to a consensus phase. At the mean-field level, where each individual interacts socially with every other, this transition occurs at the threshold value of the coupling constant [24]

$$\lambda_c^{\text{MF}}(\alpha) = \frac{\alpha}{\alpha + 1}. \quad (4)$$

In the following, we will show that, when social influence among individuals is mediated by a general social network, the threshold value of the depolarization transition can vanish, contrary to the mean-field case. We compare two different approaches: the heterogeneous mean-field (HMF) approximation [36] and the perturbation theory [37].

Heterogeneous mean-field approximation. For uncorrelated networks [38], the HMF approximation is equivalent to the so-called annealed network approximation [39], in which the adjacency matrix can be replaced by its annealed form $a_{ij} \simeq \frac{k_i k_j}{N \langle k \rangle}$ [40]. Within this approximation, one can characterize the depolarization transition in terms of a degree averaged complex global order parameter [41]

$$r(\lambda) e^{i\psi} = \frac{1}{N \langle k \rangle} \sum_{j=1}^N k_j e^{i\theta_j(\lambda)}, \quad (5)$$

where $\theta_j(\lambda)$ is computed at the steady state and $\langle \dots \rangle$ denotes the average value. $r(\lambda)$ represents the degree of consensus among the population, with $r \simeq 0$ at the polarized state and $r \simeq 1$ at the consensus state, while ψ measures the average opinion orientation at consensus. The threshold condition for the emergence of a depolarized phase can then be obtained by inserting Eq. (3) into Eq. (1) and considering the instability of the solution $r = 0$ in the self-consistent equation ensuing in the steady state. This leads to the HMF threshold (see Supplemental Material, Sec. I (SM I))

$$\lambda_c^{\text{HMF}} = \frac{\langle k \rangle}{\langle k^2 \rangle} \lambda_c^{\text{MF}}, \quad (6)$$

where λ_c^{MF} corresponds to the mean-field threshold Eq. (13).

This result, recovered also in epidemic spreading [42, 43] and synchronization phenomena [41, 44], indicates that, if the degree fluctuations are very large, the threshold can become negligibly small. In the particular case of scale-free networks [45], with a power-law degree distribution $P(k) \sim k^{-\gamma}$, for $\gamma \leq 3$ the second moment $\langle k^2 \rangle$ diverges for an infinitely large network and therefore λ_c^{HMF} tends to zero. In the present modeling framework, this result implies that, if the underlying social network is characterized by such realistic topology, any non-zero value of social influence can lead the system from polarization to consensus. Thereby, afar from the thermodynamic limit $N \rightarrow \infty$, the more heterogeneous the underlying social network, the smaller the expected threshold for the depolarization of the system. On the other hand, for $\gamma > 3$ we obtain that $\langle k^2 \rangle$ converges to a constant and therefore $\lambda_c^{\text{HMF}} > 0$. Thus, a nonzero threshold is obtained for weakly heterogeneous networks, even in the thermodynamic limit.

It is worth stressing that the depolarization threshold can vanish only if interactions are mediated by an (infinitely large) broad-tailed social network, while the threshold is finite for other network topologies and in particular in the mean-field case, when all individuals are connected all-to-all. The only exception to this general behavior holds for a uniform conviction distribution ($P(\rho)$ with exponent $\alpha = 0$), where according to Eq. (13), $\lambda_c^{\text{MF}}(\alpha = 0) = 0$. Indeed, at the mean-field level, the order parameter behaves for $\lambda \rightarrow 0$ as (see SM IA)

$$r \sim \frac{2}{\lambda} e^{-1/\lambda}. \quad (7)$$

In this special case of $\alpha = 0$ one can show that, for any degree distribution $P(k)$, a zero threshold is also recovered, indicating that a uniform conviction is a sufficient condition to obtain a vanishing threshold for any network structure; see SM IA.

Perturbation theory. Beyond the HMF approximation, one can tackle the general equation Eq. (1) relying on the spectral properties of the adjacency matrix of the social network, a method that has been proved to provide a better description of some dynamical processes on networks, such as the susceptible-infected-susceptible model of epidemic spreading [46, 47]. An analytical treatment of the model starts from the complex local order parameter [37]

$$r_j e^{i\psi_j} = \sum_{\ell=1}^N a_{j\ell} e^{i\theta_\ell(\lambda)}, \quad (8)$$

with r_j being a local measure of order and ψ_j the local average orientation, computed over the nearest neighbors of an agent. Similarly to the HMF approximation, the depolarized phase is characterized by the local consensus among the agents, i.e., $r_j > 0$. Solving for the steady state, we can then determine the threshold value of the coupling constant by letting $r_j \rightarrow 0$, which leads to (see SM II)

$$\lambda_c^{\text{P}} = \frac{\lambda_c^{\text{MF}}}{\Lambda_m}, \quad (9)$$

where Λ_m is the largest eigenvalue of the adjacency matrix. In the case of uncorrelated scale-free networks with a maximum

degree k_c , this largest eigenvalue can be estimated as [46, 48]

$$\Lambda_m \simeq \begin{cases} \langle k^2 \rangle / \langle k \rangle & 2 < \gamma < 5/2 \\ \sqrt{k_c} & \gamma > 5/2 \end{cases}. \quad (10)$$

Since k_c grows as a function of N for any γ [40, 49], the consequence of Eq. (10) is remarkable: in any uncorrelated random network with power-law distributed connectivities, the threshold value goes to zero as the network size goes to infinity. This is in contrast with the HMF approximation given by Eq. (11), since a constant threshold is not observed for $\gamma > 3$.

In order to check the previous theoretical analysis, in the following we test the different predictions of both HMF approximation and perturbation theory, λ_c^{HMF} and λ_c^{P} respectively, on synthetic and empirical networks; see SM IIIA for simulation details.

Synthetic networks. We build uncorrelated scale-free synthetic networks using the uncorrelated configuration model (UCM) [50] with a minimum degree $k_{\min} = 3$ and maximum degree $k_c = \min(N^{1/2}, N^{1/(\gamma-1)})$ [40, 49]. We consider degree exponents $\gamma = 2.5$ and $\gamma = 3.5$ to distinguish the two regimes (vanishing and non-vanishing threshold) of the HMF approximation. For simplicity, we study the case $\alpha \rightarrow \infty$, i.e., $\rho_i = 1 \forall i$, which leads to $\lambda_c^{\text{MF}} = 1$.

In Figure 2 (a) we tested the finite-size scaling of the depolarization threshold estimated by numerical simulations of the social compass model on scale-free UCM networks, by plotting it as a function of network size N . As we can see, the threshold λ_c decreases continuously for increasing N , for all values of γ . The theoretical HMF prediction, Eq. (11), depicted as a dashed line, works quite well for $\gamma = 2.5$. However, it predicts a constant threshold for $\gamma > 3$ in the thermodynamic limit, which is not compatible with numerical results for $\gamma = 3.5$.

Instead, numerical simulations are compatible with the perturbation theory and with a vanishing threshold for large N and for any γ . Indeed, in Figure 2 (b) we show the inverse of the depolarization threshold $1/\lambda_c$ as a function of the largest eigenvalue Λ_m , with the theoretical prediction of the perturbation theory, Eq. (9), depicted as a black dashed line. As we can see, the numerical results are recovered with good accuracy by the theoretical expression, which predicts the correct scaling of the numerical threshold up to a constant multiplicative factor. We notice, however, that the agreement between theory and simulations is better for $\gamma = 2.5$ than for $\gamma = 3.5$, in which the perturbation theory prediction is recovered for the largest values of Λ_m , corresponding to large network sizes. Thus, we can attribute the deviation of the case $\gamma = 3.5$ from the theory to finite-size effects.

One could argue that the validity of the perturbation theory is contingent to the assumption of a local order parameter, Eq. (19), being close to zero in the vicinity of the polarized state. The vanishing of the local order parameter can only be achieved when it is computed over a sufficiently large number of nearest neighbors. Thus, one might expect that perturbation theory would work better for networks with larger connectivity, i.e., with a larger average degree. The average degree grows in UCM networks with decreasing γ , so we could expect that

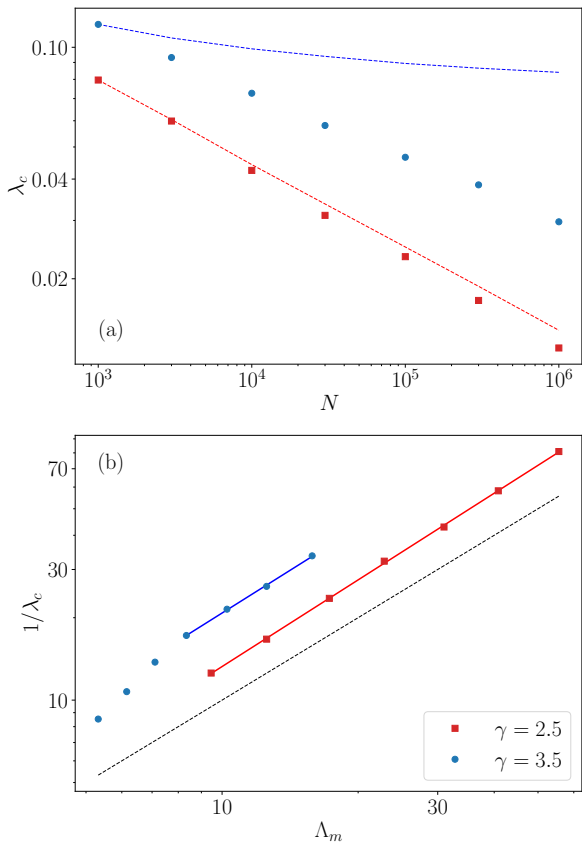


Figure 2. **Depolarization threshold on synthetic networks.** (a) Numerical threshold λ_c as a function of N for scale-free synthetic networks with different exponents γ . The dashed lines, representing the theoretical prediction of the HMF theory, have been arbitrarily shifted to ease comparison with numerical data. (b) Inverse of the numerical threshold $1/\lambda_c$ as a function of Λ_m for different values of γ . The dashed line represents the theoretical prediction of the perturbation theory. Solid lines represent power regression $1/\lambda_c \sim \Lambda_m^a$, with $a = 1.05 \pm 0.01$ for $\gamma = 2.5$ and $a = 1.04 \pm 0.02$ for $\gamma = 3.5$. Due to finite-size effects, the power regression for $\gamma = 3.5$ is performed over the four largest network sizes. Initial opinions: constant conviction $\rho = 1$, given by Eq. (2) for $\alpha \rightarrow \infty$, and bimodal orientation, given by Eq. (3). Each point is averaged over 100 UCM network realizations, being the eigenvalue of the adjacency matrix computed as the mean value of all the realizations. Error bars are smaller than symbols.

perturbation theory prediction is more accurate for smaller values of γ . We checked that this intuition is not correct by performing numerical simulations on UCM networks with $\gamma = 3.5$ and a larger average degree, obtained by imposing $k_{\min} = 10$. The results (not shown) indicate that the performance of the perturbation theory is not increased by a larger average degree. We conclude then that perturbation theory is valid in general for scale-free networks with any exponent γ in the thermodynamic limit, corresponding to large network size and large largest eigenvalue.

Empirical networks. To check the validity of our theoretical prediction in a more general scenario than the synthetic UCM model, we performed simulations of the social compass model

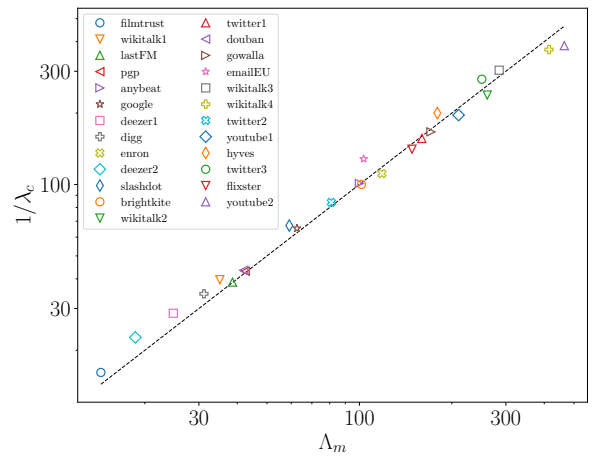


Figure 3. **Depolarization threshold on empirical social networks.** Inverse of the numerical threshold $1/\lambda_c$ as a function of Λ_m for different empirical social networks. The dashed line represents the theoretical prediction of the perturbation theory. Initial opinions: constant conviction $\rho = 1$, given by Eq. (2) with $\alpha = \infty$, and bimodal orientation, given by Eq. (3). Each point is averaged over 10 initial orientation distributions. Error bars are smaller than symbols.

on a set of 25 real social networks representing user-user interactions in online networking platforms, such as direct messages or friendship connections. Networks range in sizes between $N = 10^3$ and $N = 3 \times 10^6$ and have different levels of degree heterogeneity; see SM III B for details. In the simulations, we consider again the case of a constant conviction ($\alpha \rightarrow \infty$), so that $\lambda_c^{\text{MF}} = 1$. In Figure 3 we present a scatter plot of the inverse of the numerically estimated thresholds $1/\lambda_c$ as a function of the largest eigenvalue Λ_m computed for each network. As we can see, the perturbation theory provides an excellent prediction of the threshold value for all the different empirical networks considered, confirming the linear scaling, Eq. (9), depicted as a black dashed line.

Discussion. Here we showed that the depolarization threshold of the social compass model, within a population characterized by heterogeneous social interactions, can be very small. This indicates that even a weak social influence among individuals may be able to trigger consensus. This result is particularly relevant since most empirical social networks are highly heterogeneous, so it could be easier to reduce opinion polarization in these realistic settings. A smaller depolarization threshold for increasingly heterogeneous social networks can be understood by the presence of highly connected nodes (hubs) extending their social influence to a large number of nodes, while the social influence they receive from those neighbors is averaged down. Therefore, the presence of hubs promotes the formation of consensus, decreasing the depolarization threshold.

It is important to discuss if these findings can generalize beyond the specific case of the social compass model. To this aim, we considered different definitions of the model by replacing the sine in the first term of Eq. (1) (describing the tendency of individuals to remain close to their preferred orientation) with similar functions. One should consider odd functions in order to preserve the correct representation of the orientations

in the polar plane. Furthermore, one needs monotonic functions leading to a higher response if the orientation difference is greater. Finally, it is essential to ensure finite outputs from the function to avoid diverging results. These requirements describe a potential well for the orientation θ centered around the preferred orientation φ . We tested the behavior of the model by using functions respecting these requirements, such as the hyperbolic tangent $\tanh(\varphi_i - \theta_i)$ or even the simple difference $\varphi_i - \theta_i$, finding identical results, i.e., a vanishing threshold in the thermodynamic limit.

A different case holds for the second term in Eq. (1), modeling social influence among individuals. In order to capture the nature of the polar coordinates representing the opinions on two topics, the interaction term must be periodic on the angular difference $\theta_j - \theta_i$ for both angles θ_j and θ_i . In terms of a harmonic decomposition [51, 52], it is clear that the sinusoidal form chosen in both the Kuramoto model [51] and the social compass model is the simplest one fulfilling the periodicity condition. Other non-periodic functions are not allowed, since they do not lead to a phase transition between two well-differentiated regimes.

However, note that despite the coupling term being the same

in both models, each model's behavior on scale-free networks is notably different from the other in the thermodynamic limit. Indeed, the depolarization threshold of the social compass model vanishes regardless of the degree heterogeneity, following the predictions of perturbation theory, Eq. (9), while the synchronization threshold of the Kuramoto model remains constant for $\gamma > 3$ [53], as it is predicted by a HMF theory analogous to Eq. (11). This is due to the different nature of the variables considered: while in the Kuramoto model the variables θ_i , which represent the phases of local oscillators, become locked and rotate in synchrony for sufficiently large interactions, in the social compass model θ_i , which represent an orientation, reach a steady, constant state at large times.

ACKNOWLEDGMENTS

We acknowledge financial support from the Spanish MCIN/AEI/10.13039/501100011033, under Project No.PID2019-106290GB-C21.

-
- [1] J. McCoy, T. Rahman, and M. Somer, *American Behavioral Scientist* **62**, 16 (2018).
- [2] M. D. Vicario, W. Quattrociochi, A. Scala, and F. Zollo, *ACM Trans. Web* **13**, 10:1 (2019).
- [3] A. Vinokur and E. Burnstein, *Journal of Personality and Social Psychology* **36**, 872 (1978).
- [4] A. G. Miller, J. W. McHoskey, C. M. Bane, and T. G. Dowd, *Journal of Personality and Social Psychology* **64**, 561 (1993).
- [5] A. Matakos, E. Terzi, and P. Tsaparas, *Data Min Knowl Disc* **31**, 1480 (2017).
- [6] C. Musco, C. Musco, and C. E. Tsourakakis, in *Proceedings of the 2018 World Wide Web Conference*, WWW '18 (International World Wide Web Conferences Steering Committee, Republic and Canton of Geneva, CHE, 2018) pp. 369–378.
- [7] S. Ballester, L. Getoor, D. G. Goldstein, and D. J. Watts, *Proceedings of the National Academy of Sciences* **118**, e2112552118 (2021).
- [8] R. Axelrod, *Journal of Conflict Resolution* **41**, 203 (1997).
- [9] F. Baumann, P. Lorenz-Spreen, I. M. Sokolov, and M. Starnini, *Phys. Rev. Lett.* **124**, 048301 (2020).
- [10] G. Deffuant, D. Neau, F. Amblard, and G. Weisbuch, *Adv. Complex Syst.* **03**, 87 (2000).
- [11] R. Hegselmann and U. Krause, *Journal of Artificial Societies and Social Simulation* **5**, 1 (2002).
- [12] T. V. Martins, M. Pineda, and R. Toral, *EPL* **91**, 48003 (2010).
- [13] C. Crawford, L. Brooks, and S. Sen, in *Proceedings of the 2013 international conference on Autonomous agents and multi-agent systems*, AAMAS '13 (International Foundation for Autonomous Agents and Multiagent Systems, Richland, SC, 2013) pp. 1225–1226.
- [14] K. Sznajd-Weron and J. Sznajd, *Int. J. Mod. Phys. C* **11**, 1157 (2000).
- [15] D. López-Pintado and D. J. Watts, *Rationality and Society* **20**, 399 (2008).
- [16] S. E. Parsegov, A. V. Proskurnikov, R. Tempo, and N. E. Friedkin, *IEEE Transactions on Automatic Control* **62**, 2270 (2017).
- [17] S. Schweighofer, D. Garcia, and F. Schweitzer, *Chaos* **30**, 093139 (2020).
- [18] T. Chen, X. Yin, J. Yang, G. Cong, and G. Li, *Axioms* **10**, 270 (2021).
- [19] D. Baldassarri and A. Gelman, *AJS* **114**, 408 (2008).
- [20] K. Benoit and M. Laver, *European Union Politics* **13**, 194 (2012).
- [21] D. DellaPosta, Y. Shi, and M. Macy, *American Journal of Sociology* **120**, 1473 (2015).
- [22] F. Falck, J. Marsteller, N. Stoehr, S. Maucher, J. Ren, A. Thahammer, A. Rettinger, and R. Studer, *Policy & Internet* **12**, 367 (2020).
- [23] K. O'Brien, W. Forrest, D. Lynott, and M. Daly, *PLOS ONE* **8**, e77552 (2013).
- [24] J. Ojer, M. Starnini, and R. Pastor-Satorras, *Phys. Rev. Lett.* **130**, 207401 (2023).
- [25] J.-M. Esteban and D. Ray, *Econometrica* **62**, 819 (1994).
- [26] M. H. Degroot, *Journal of the American Statistical Association* **69**, 118 (1974).
- [27] <http://www.politicalcompass.org>.
- [28] C. B. Currin, S. V. Vera, and A. Khaledi-Nasab, *Sci Rep* **12**, 9234 (2022).
- [29] R. Pal, A. Kumar, and M. S. Santhanam, "Depolarization of opinions on social networks through random nudges," (2023), [arXiv:2212.06920v2 \[physics.soc-ph\]](https://arxiv.org/abs/2212.06920v2).
- [30] P. Sobkowicz, *Entropy* **25**, 568 (2023).
- [31] F. Baumann, P. Lorenz-Spreen, I. M. Sokolov, and M. Starnini, *Phys. Rev. X* **11**, 011012 (2021).
- [32] A. Barrat, M. Barthlemy, and A. Vespignani, *Dynamical Processes on Complex Networks*, 1st ed. (Cambridge University Press, USA, 2008).
- [33] P. DiMaggio, J. Evans, and B. Bryson, *American Journal of Sociology* **102**, 690 (1996).
- [34] M. Jackson, *Social and Economic Networks* (Princeton University Press, Princeton, 2010).

- [35] M. Newman, *Networks: An Introduction* (Oxford University Press, Inc., New York, NY, USA, 2010).
- [36] R. Pastor-Satorras and A. Vespignani, *Phys. Rev. Lett.* **86**, 3200 (2001).
- [37] J. G. Restrepo, E. Ott, and B. R. Hunt, *Phys. Rev. E* **71**, 036151 (2005).
- [38] M. E. J. Newman, *Phys. Rev. Lett.* **89**, 208701 (2002).
- [39] S. N. Dorogovtsev, A. V. Goltsev, and J. F. F. Mendes, *Rev. Mod. Phys.* **80**, 1275 (2008).
- [40] M. Boguñá, C. Castellano, and R. Pastor-Satorras, *Phys. Rev. E* **79**, 036110 (2009).
- [41] T. Ichinomiya, *Phys. Rev. E* **70**, 026116 (2004).
- [42] M. Boguñá and R. Pastor-Satorras, *Phys. Rev. E* **66**, 047104 (2002).
- [43] M. Boguñá, R. Pastor-Satorras, and A. Vespignani, *Phys. Rev. Lett.* **90**, 028701 (2003).
- [44] D.-S. Lee, *Phys. Rev. E* **72**, 026208 (2005).
- [45] A.-L. Barabási and R. Albert, *Science* **286**, 509 (1999).
- [46] C. Castellano and R. Pastor-Satorras, *Phys. Rev. Lett.* **105**, 218701 (2010).
- [47] S. C. Ferreira, C. Castellano, and R. Pastor-Satorras, *Phys. Rev. E* **86**, 041125 (2012).
- [48] F. Chung, L. Lu, and V. Vu, *Proceedings of the National Academy of Sciences* **100**, 6313 (2003).
- [49] M. Boguñá, R. Pastor-Satorras, and A. Vespignani, *Euro. Phys. J. B* **38**, 205 (2004).
- [50] M. Catanzaro, M. Boguñá, and R. Pastor-Satorras, *Phys. Rev. E* **71**, 027103 (2005).
- [51] Y. Kuramoto, in *International Symposium on Mathematical Problems in Theoretical Physics*, Lecture Notes in Physics, edited by H. Araki (Springer, Berlin, Heidelberg, 1975) pp. 420–422.
- [52] S. H. Strogatz, *Physica D: Nonlinear Phenomena* **143**, 1 (2000).
- [53] T. Peron, B. Messias F. de Resende, A. S. Mata, F. A. Rodrigues, and Y. Moreno, *Phys. Rev. E* **100**, 042302 (2019).
- [54] R. Pastor-Satorras, A. Vázquez, and A. Vespignani, *Phys. Rev. Lett.* **87**, 258701 (2001).
- [55] P. Virtanen, R. Gommers, T. E. Oliphant, M. Haberland, T. Reddy, D. Cournapeau, E. Burovski, P. Peterson, W. Weckesser, J. Bright, S. J. van der Walt, M. Brett, J. Wilson, K. J. Millman, N. Mayorov, A. R. J. Nelson, E. Jones, R. Kern, E. Larson, C. J. Carey, Í. Polat, Y. Feng, E. W. Moore, J. VanderPlas, D. Laxalde, J. Perktold, R. Cimrman, I. Henriksen, E. A. Quintero, C. R. Harris, A. M. Archibald, A. H. Ribeiro, F. Pedregosa, P. van Mulbregt, and SciPy 1.0 Contributors, *Nature Methods* **17**, 261 (2020).
- [56] J. A. Acebrón, L. L. Bonilla, C. J. P. Vicente, F. Ritort, and R. Spigler, *Reviews of Modern Physics* **77**, 137 (2005).
- [57] S.-H. Yook and Y. Kim, *Phys. Rev. E* **97**, 042317 (2018).
- [58] G. Guo, J. Zhang, and N. Yorke-Smith, in *Proceedings of the Twenty-Third international joint conference on Artificial Intelligence*, IJCAI '13 (AAAI Press, Beijing, China, 2013) pp. 2619–2625.
- [59] J. Sun, J. Kunegis, and S. Staab, in *2016 IEEE 16th International Conference on Data Mining Workshops (ICDMW)* (2016) pp. 128–135, iSSN: 2375-9259.
- [60] B. Rozemberczki and R. Sarkar, in *Proceedings of the 29th ACM International Conference on Information & Knowledge Management*, CIKM '20 (Association for Computing Machinery, New York, NY, USA, 2020) pp. 1325–1334.
- [61] M. Boguñá, R. Pastor-Satorras, A. Díaz-Guilera, and A. Arenas, *Phys. Rev. E* **70**, 056122 (2004).
- [62] M. Fire, R. Puzis, and Y. Elovici, in *Handbook of Computational Approaches to Counterterrorism*, edited by V. Subrahmanian (Springer, New York, NY, 2013) pp. 283–300.
- [63] J. McAuley and J. Leskovec, in *Proceedings of the 25th International Conference on Neural Information Processing Systems - Volume 1*, NIPS'12 (Curran Associates Inc., Red Hook, NY, USA, 2012) pp. 539–547.
- [64] M. De Choudhury, H. Sundaram, A. John, and D. D. Seligmann, in *2009 International Conference on Computational Science and Engineering*, Vol. 4 (2009) pp. 151–158.
- [65] M. W. Mahoney, A. Dasgupta, J. Leskovec, and K. J. Lang, *Internet Mathematics* **6** (2009).
- [66] B. Rozemberczki, R. Davies, R. Sarkar, and C. Sutton, in *Proceedings of the 2019 IEEE/ACM International Conference on Advances in Social Networks Analysis and Mining*, ASONAM '19 (Association for Computing Machinery, New York, NY, USA, 2020) pp. 65–72.
- [67] V. Gómez, A. Kaltenbrunner, and V. López, in *Proceedings of the 17th international conference on World Wide Web*, WWW '08 (Association for Computing Machinery, New York, NY, USA, 2008) pp. 645–654.
- [68] E. Cho, S. A. Myers, and J. Leskovec, in *Proceedings of the 17th ACM SIGKDD international conference on Knowledge discovery and data mining*, KDD '11 (Association for Computing Machinery, New York, NY, USA, 2011) pp. 1082–1090.
- [69] E. Omodei, M. D. De Domenico, and A. Arenas, *Front. Phys.* **3** (2015).
- [70] R. Zafarani and H. Liu, “Social computing data repository at ASU,” (2009).
- [71] J. Leskovec, J. Kleinberg, and C. Faloutsos, *ACM Trans. Knowl. Discov. Data* **1**, 2 (2007).
- [72] M. D. Choudhury, Y.-R. Lin, H. Sundaram, K. S. Candan, L. Xie, and A. Kelliher, in *Proceedings of the Fourth International Conference on Weblogs and Social Media, ICWSM 2010, Washington, DC, USA, May 23-26, 2010*, edited by W. W. Cohen and S. Gosling (The AAAI Press, 2010).
- [73] J. Yang and J. Leskovec, *Knowl Inf Syst* **42**, 181 (2015).
- [74] M. De Domenico and E. G. Altmann, *Sci Rep* **10**, 4629 (2020).
- [75] A. Mislove, M. Marcon, K. P. Gummadi, P. Druschel, and B. Bhattacharjee, in *Proceedings of the 7th ACM SIGCOMM conference on Internet measurement*, IMC '07 (Association for Computing Machinery, New York, NY, USA, 2007) pp. 29–42.

Supplemental Material

I. HETEROGENEOUS MEAN-FIELD APPROXIMATION

The heterogeneous mean-field (HMF) approximation consists in disregarding the actual structure of the network and keeping only a statistical description based on the degree distribution $P(k)$ [36], giving the probability that a randomly chosen agent has degree k (is connected to k other agents), and the conditional probability $P(k'|k)$ that a random connection from an agent of degree k points to an agent of degree k' [54]. In the simplest case of uncorrelated networks [38], where the conditional probability can be written as $P_{\text{un}}(k'|k) = k'P(k')/\langle k \rangle$ [39, 54], the HMF approximation is equivalent to the so-called annealed network approximation [39], in which the adjacency matrix can be replaced by its annealed form [40]

$$a_{ij} \simeq \bar{a}_{ij} = \frac{k_i k_j}{N \langle k \rangle}. \quad (1)$$

Inserting this expression into the general model equation, Eq. (1) of the main text, we obtain

$$\dot{\theta}_i(t) = \rho_i \sin[\varphi_i - \theta_i(t)] + \frac{\lambda k_i}{N \langle k \rangle} \sum_{j=1}^N k_j \sin[\theta_j(t) - \theta_i(t)]. \quad (2)$$

We can introduce now the degree averaged complex global order parameter [41]

$$r(\lambda) e^{i\psi} = \frac{1}{N \langle k \rangle} \sum_{j=1}^N k_j e^{i\theta_j(\lambda)}, \quad (3)$$

where the mean-field values r and ψ represent the degree of consensus among the population and the average orientation of the agents, respectively. Considering that [41]

$$\text{Im} \left\{ r e^{i(\psi - \theta_j)} \right\} = r \sin(\psi - \theta_j) = \text{Im} \left\{ \frac{1}{N \langle k \rangle} \sum_{\ell} k_{\ell} e^{i(\theta_{\ell} - \theta_j)} \right\} = \frac{1}{N \langle k \rangle} \sum_{\ell} k_{\ell} \sin(\theta_{\ell} - \theta_j), \quad (4)$$

we can write Eq. (2) as

$$\dot{\theta}_i = \rho_i \sin(\varphi_i - \theta_i) + \lambda k_i r \sin(\psi - \theta_i), \quad (5)$$

in which the (apparently independent) orientation variables are coupled by means of the mean-field quantities r and ψ . Solving the previous equation for the steady state, we can write the orientation of each agent as a function of r and ψ , namely [24]

$$\theta_i(r, \psi) = \arctan \left(\frac{\lambda k_i r \sin(\psi) + \rho_i \sin(\varphi_i)}{\lambda k_i r \cos(\psi) + \rho_i \cos(\varphi_i)} \right). \quad (6)$$

Inserting this expression into the degree averaged complex global order parameter Eq. (3), averaging over the distributions $P(\rho)$ and $P(\varphi)$ and taking the continuous degree approximation, we can write [24, 41]

$$\begin{aligned} r &= \frac{1}{\langle k \rangle} \int dk k P(k) \int d\rho P(\rho) \int d\varphi P(\varphi) e^{i[\theta(r, \psi) - \psi]} \\ &= \frac{1}{\langle k \rangle} \int dk \int d\rho \int d\varphi \frac{k P(k) P(\rho) P(\varphi) [\lambda k r + \rho e^{i(\varphi - \psi)}]}{\sqrt{(\lambda k r)^2 + 2\lambda k r \rho \cos(\varphi - \psi) + \rho^2}} \equiv I_{\text{HMF}}(\lambda, r, \psi). \end{aligned} \quad (7)$$

Taking the real and imaginary parts of this expression, we find the relations

$$r = \text{Re} \{ I_{\text{HMF}}(\lambda, r, \psi) \} \equiv I_r(\lambda, r, \psi), \quad (8)$$

$$0 = \text{Im} \{ I_{\text{HMF}}(\lambda, r, \psi) \} \equiv I_{\psi}(\lambda, r, \psi). \quad (9)$$

The first equation defines the order parameter r self-consistently, while the second relation allows us to compute the value of the average orientation ψ .

We can estimate the value of the threshold by looking at the condition for the onset of instability of the solution $r = 0$, namely

$$\left. \frac{\partial I_r(\lambda, r, \psi)}{\partial r} \right|_{r=0} = \frac{1}{\langle k \rangle} \int dk k P(k) \int d\rho P(\rho) \int d\varphi P(\varphi) \frac{\lambda k}{\rho} \sin^2(\varphi - \psi) \geq 1. \quad (10)$$

This condition translates into the threshold

$$\lambda_c^{\text{HMF}} = \frac{\langle k \rangle}{\langle k^2 \rangle} \lambda_c^{\text{MF}}, \quad (11)$$

where

$$\lambda_c^{\text{MF}} = \frac{1}{\int_0^\infty d\rho \frac{P(\rho)}{\rho} \int_{-\pi}^\pi d\varphi P(\varphi) \sin^2(\varphi - \psi)} \quad (12)$$

is the depolarization threshold at the mean-field level [24].

A. Threshold zero for a uniform conviction

At the mean-field level, for a power-law-distributed conviction $P(\rho) \sim \rho^\alpha$ and a bimodal $P(\varphi)$, Eqs. (2) and (3) of the main text respectively, the depolarization threshold Eq. (12) takes the form [24]

$$\lambda_c^{\text{MF}}(\alpha) = \frac{\alpha}{\alpha + 1}, \quad (13)$$

which vanishes for a uniform conviction distribution with exponent $\alpha = 0$. Indeed, in the case of agents connected all-to-all, the self-consistent equation for the order parameter Eq. (8) reads

$$r = \int_0^1 d\rho \frac{\lambda r}{\sqrt{(\lambda r)^2 + \rho^2}} = \lambda r \operatorname{arctanh} \left(\frac{1}{\sqrt{(\lambda r)^2 + 1}} \right). \quad (14)$$

Apart from the solution $r = 0$, corresponding to the polarized state, we find the non-zero solution

$$r(\lambda) = \frac{1}{\lambda \sinh \left(\frac{1}{\lambda} \right)}, \quad (15)$$

which vanishes only for $\lambda = 0$, indicating a null threshold. The asymptotic behaviors of the order parameter are then

$$r(\lambda) \sim \begin{cases} \frac{2}{\lambda} e^{-1/\lambda} & \lambda \rightarrow 0 \\ \frac{1}{1 + \frac{1}{6\lambda^2}} & \lambda \rightarrow \infty \end{cases}. \quad (16)$$

Interestingly, the special case of a uniform conviction distribution leads to a self-consistent equation Eq. (8) for a degree distribution $P(k)$ that follows as

$$r = \frac{1}{\langle k \rangle} \int k^2 P(k) \lambda r \operatorname{arctanh} \left(\frac{1}{\sqrt{(\lambda k r)^2 + 1}} \right) dk \equiv f(r). \quad (17)$$

While the integral cannot be performed in the general case, we can obtain the threshold as the value of λ above which a non-zero solution exists. Using standard geometric arguments, we can see that a non-zero solution exists when the right-hand side of Eq. (17) fulfills the condition $f'(r)|_{r=0} \geq 1$. We have

$$f'(r) = \frac{1}{\langle k \rangle} \int k^2 P(k) \lambda \left[\operatorname{arctanh} \left(\frac{1}{\sqrt{(\lambda k r)^2 + 1}} \right) - \frac{1}{(\lambda k r)^2 + 1} \right] dk. \quad (18)$$

In the limit $r \rightarrow 0$, the argument of the $\operatorname{arctanh}$ tends to 1 and this function thus diverges. Therefore, $\lim_{r \rightarrow 0} f'(r) = \infty$ for any network structure, implying that $f'(r)|_{r=0}$ is larger than 1 for any value of λ , which indicates that $\lambda_c^{\text{HMF}} = 0$.

II. PERTURBATION THEORY

For social interactions mediated by a general network, an analytical treatment of the model starts from the complex local order parameter [37]

$$r_j e^{i\psi_j} = \sum_{\ell=1}^N a_{j\ell} e^{i\theta_\ell(\lambda)}, \quad (19)$$

with r_j being a local measure of order and ψ_j the local average orientation, computed over the nearest neighbors of an agent. Defining now $\Delta\theta_i \equiv \theta_i - \psi_i$ and $\Delta\varphi_i \equiv \varphi_i - \psi_i$, we can write the previous equation as

$$r_j = \sum_{\ell=1}^N a_{j\ell} e^{i\Delta\theta_\ell} e^{i(\psi_\ell - \psi_j)}. \quad (20)$$

Similarly to Eq. (5), the general model equation can be coupled as

$$\Delta\dot{\theta}_i = \rho_i \sin(\Delta\varphi_i - \Delta\theta_i) - \lambda r_i \sin(\Delta\theta_i). \quad (21)$$

The steady state is then given by

$$\Delta\theta_i = \arctan\left(\frac{\rho_i \sin(\Delta\varphi_i)}{\lambda r_i + \rho_i \cos(\Delta\varphi_i)}\right). \quad (22)$$

Inserting this expression into Eq. (20), we obtain [37]

$$r_i = \sum_{\rho_j} \sum_{\varphi_j} \frac{a_{ij} \cos(\psi_j - \psi_i) [\lambda r_j + \rho_j \cos(\Delta\varphi_j)]}{\sqrt{(\lambda r_j)^2 + 2\lambda r_j \rho_j \cos(\Delta\varphi_j) + \rho_j^2}} - \sum_{\rho_j} \sum_{\varphi_j} \frac{a_{ij} \sin(\psi_j - \psi_i) \rho_j \sin(\Delta\varphi_j)}{\sqrt{(\lambda r_j)^2 + 2\lambda r_j \rho_j \cos(\Delta\varphi_j) + \rho_j^2}}, \quad (23)$$

$$0 = \sum_{\rho_j} \sum_{\varphi_j} \frac{a_{ij} \sin(\psi_j - \psi_i) [\lambda r_j + \rho_j \cos(\Delta\varphi_j)]}{\sqrt{(\lambda r_j)^2 + 2\lambda r_j \rho_j \cos(\Delta\varphi_j) + \rho_j^2}} + \sum_{\rho_j} \sum_{\varphi_j} \frac{a_{ij} \cos(\psi_j - \psi_i) \rho_j \sin(\Delta\varphi_j)}{\sqrt{(\lambda r_j)^2 + 2\lambda r_j \rho_j \cos(\Delta\varphi_j) + \rho_j^2}}, \quad (24)$$

for the real and imaginary parts, respectively. For a bimodal $P(\varphi)$, Eq. (3) of the main text, one half of the population holds $\varphi_i = 0$ (state 1), whereas the other half $\varphi_i = \pi$ (state 2). Near the transition to consensus, if the number of connections per agent is large, one half of the neighbors will likely be at state 1 ($\theta_j = 0$) and the other half at state 2 ($\theta_j = \pi$). Therefore, $\psi_i = \pi/2 \forall i$ such that $\psi_j - \psi_i = 0$. Eqs. (23) and (24) are then reduced to

$$r_i = \sum_{\rho_j} \sum_{\varphi_j} \frac{a_{ij} [\lambda r_j + \rho_j \cos(\Delta\varphi_j)]}{\sqrt{(\lambda r_j)^2 + 2\lambda r_j \rho_j \cos(\Delta\varphi_j) + \rho_j^2}}, \quad (25)$$

$$0 = \sum_{\rho_j} \sum_{\varphi_j} \frac{a_{ij} \rho_j \sin(\Delta\varphi_j)}{\sqrt{(\lambda r_j)^2 + 2\lambda r_j \rho_j \cos(\Delta\varphi_j) + \rho_j^2}}, \quad (26)$$

respectively. Moreover, for the neighbors at state 1 $\Delta\varphi_j = -\pi/2$, whereas for the ones at state 2 $\Delta\varphi_j = \pi/2$. Hence, Eq. (26) for the imaginary part is satisfied. For the real part, approximating the sum of conviction as an integral and summing over all the agents, we obtain

$$r_i = \sum_{j=1}^N a_{ij} \int d\rho P(\rho) \frac{\lambda r_j}{\sqrt{(\lambda r_j)^2 + \rho^2}}. \quad (27)$$

We can determine the threshold value of λ by letting $r_i \rightarrow 0$. Expanding the right-hand side of the previous equation at first-order, we obtain

$$r_i^{(0)} = \frac{\lambda}{\lambda_c^{\text{MF}}} \sum_{j=1}^N a_{ij} r_j^{(0)}, \quad (28)$$

where, for a power-law-distributed conviction, Eq. (2) of the main text, λ_c^{MF} is the threshold value Eq. (13) at the mean-field level. We thus identify the depolarization threshold of the coupling constant with the largest eigenvalue Λ_m of the adjacency matrix [37], obtaining

$$\lambda_c^{\text{P}} = \frac{\lambda_c^{\text{MF}}}{\Lambda_m}. \quad (29)$$

III. NUMERICAL RESULTS

In order to verify the validity of our theoretical predictions, we performed extensive numerical simulations of the model on both synthetic and empirical social networks.

A. Simulation details

Simulations are performed by numerically integrating the general model equation, Eq. (1) of the main text, starting from an initial condition $\theta_i(0) = \varphi_i + 10^{-3}\epsilon$, where $\epsilon \in U(-1, 1)$. The numerical integration is performed using the adaptive stepsize algorithm in the function `odeint` of the Python scientific computing package `scipy` [55]. We choose as global order parameter the function given by [56]

$$r(\lambda)e^{i\psi} = \frac{1}{N} \sum_{j=1}^N e^{i\theta_j(\lambda)}, \quad (30)$$

since the degree averaged version in Eq. (3) can overestimate the degree of consensus in the polarized phase due to finite-size effects [57]. The order parameter is evaluated at the steady state of the numerical integration, which we define by a difference between consecutive time steps $\Delta r < 10^{-8}$. We determined the threshold λ_c as the smallest value of λ for which a degree of consensus $r > 10^{-6}$ is reached.

B. Empirical networks

In the following we briefly describe the different empirical social networks used in our work; in Table I we summarize their main topological properties. Although some of these networks have a directed nature [35], in our simulations we have symmetrized, rendering them effectively undirected.

1. **filmtrust** [58]: user-user trust network of the FilmTrust website, through which each person can recommend movies to their friends.
2. **wikitalk1** [59]: communication network of the Welsh Wikipedia website edition, where nodes represent users and edges online messages.
3. **lastFM** [60]: friendship network of the Last.fm music website, where nodes represent users from Asian countries and edges mutual follower relationships between them.
4. **pgp** [61]: interaction network of the Pretty Good Privacy encryption algorithm, through which users share confidential information.
5. **anybeat** [62]: friendship network of the AnyBeat online community, where nodes represent users and edges follower relationships between them.
6. **google** [63]: user-user network of the Google+ service, where nodes represent users and edges follower relationships between them.
7. **deezer1** [60]: friendship network of the Deezer music streaming service, where nodes represent users from European countries and edges mutual follower relationships between them.
8. **digg** [64]: interaction network of the news website Digg, where nodes represent users and edges replies between them.
9. **enron** [65]: communication network of the Enron email dataset, where nodes represent email addresses and edges the emails sent between them.
10. **deezer2** [66]: friendship network of the Deezer music streaming service, where nodes represent users from Romania and edges mutual follower relationships between them.
11. **slashdot** [67]: interaction network of the technology website Slashdot, where nodes represent users and edges replies between them.
12. **brightkite** [68]: friendship network of the Brightkite location-based website, where nodes represent users and edges mutual follower relationships between them.
13. **wikitalk2** [59]: communication network of the Catalan Wikipedia website edition, where nodes represent users and edges online messages.
14. **twitter1** [69]: interaction network of Twitter service during the 2014 People's Climate March, where nodes represent users and edges retweets, mentions and replies between them.

15. **douban** [70]: user-user recommendation network of the Douban online website, through which each person can create content with their followers.
16. **gowalla** [68]: friendship network of the Gowalla location-based service, where nodes represent users and edges mutual follower relationships between them.
17. **emailEU** [71]: communication network of an European research institution, where nodes represent email addresses and edges the emails sent between them.
18. **wikitalk3** [59]: communication network of the Vietnamese Wikipedia website edition, where nodes represent users and edges online messages.
19. **wikitalk4** [59]: communication network of the Japanese Wikipedia website edition, where nodes represent users and edges online messages.
20. **twitter2** [72]: friendship network of Twitter service, where nodes represent users and edges follower relationships between them.
21. **youtube1** [73]: friendship network of the YouTube video-sharing website, where nodes represent users and edges mutual follower relationships between them.
22. **hyves** [70]: friendship network of the Hyves website, where nodes represent users and edges mutual follower relationships between them.
23. **twitter3** [74]: interaction network of Twitter service during the 2015 Paris attacks, where nodes represent users and edges retweets, mentions and replies between them.
24. **flixfster** [70]: friendship network of the Flixster movie rating site, where nodes represent users and edges mutual follower relationships between them.
25. **youtube2** [75]: friendship network of the YouTube video-sharing website, where nodes represent users and edges mutual follower relationships between them.

Network	N	$\langle k \rangle$	χ	Λ_m	Kind
filmtrust	874	3.00	2.33	14.4	Directed
wikitalk1	2233	3.47	57.12	35.1	Directed
lastFM	7624	7.29	2.49	38.6	Undirected
pgp	10680	4.55	3.15	42.4	Undirected
anybeat	12645	7.77	49.04	99.9	Directed
google	23628	3.32	112.65	62.6	Directed
deezer1	28281	6.56	1.47	24.8	Undirected
digg	30398	5.64	3.97	31.2	Directed
enron	36692	10.02	12.98	118.4	Undirected
deezer2	41773	6.02	0.84	18.6	Undirected
slashdot	51083	4.58	16.80	59.1	Directed
brightkite	58228	7.35	7.66	101.5	Undirected
wikitalk2	79736	4.60	2307.27	260.8	Directed
twitter1	102439	6.41	131.14	159.8	Directed
douban	154908	4.22	7.74	42.0	Undirected
gowalla	196591	9.67	30.71	170.9	Undirected
emailEU	265214	2.75	194.00	103.2	Directed
wikitalk3	338714	2.46	6711.22	285.2	Directed
wikitalk4	397635	3.14	9642.97	414.5	Directed
twitter2	465017	3.58	62.19	81.0	Directed
youtube1	1134890	5.27	92.93	210.4	Undirected
hyves	1402673	3.96	130.82	179.3	Undirected
twitter3	1896221	3.90	537.53	250.4	Directed
flixfster	2523386	6.28	34.08	148.3	Undirected
youtube2	3223589	5.82	485.75	464.9	Undirected

Table I. Topological properties of the real social networks considered: Network size N ; average degree $\langle k \rangle$; heterogeneity parameter $\chi = \langle k^2 \rangle / \langle k \rangle^2 - 1$; largest eigenvalue Λ_m ; kind (directed or undirected).